

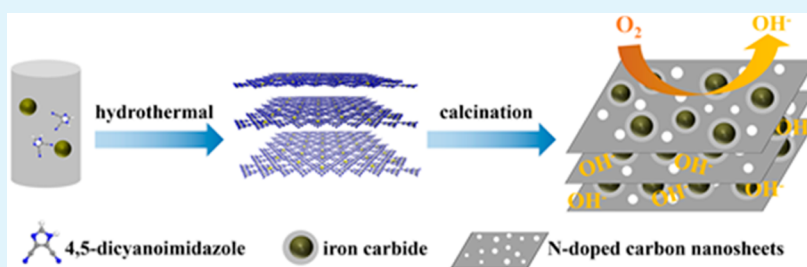
Lamellar Metal Organic Framework-Derived Fe–N–C Non-Noble Electrocatalysts with Bimodal Porosity for Efficient Oxygen Reduction

Zhongtao Li,[†] Hongdi Sun,[†] Liangqin Wei,[†] Wen-Jie Jiang,^{*,‡} Mingbo Wu,^{*,†} and Jin-Song Hu^{*,‡,⊙}

[†]State Key Laboratory of Heavy Oil Processing, School of Chemical Engineering, China University of Petroleum, Qingdao 266580, China

[‡]Beijing National Laboratory for Molecular Sciences and CAS Key Laboratory of Molecular Nanostructure and Nanotechnology, Institute of Chemistry, Chinese Academy of Sciences, 2 North First Street, Zhongguancun, Beijing 100190, China

S Supporting Information



ABSTRACT: Developing highly efficient and stable non-Pt electrocatalysts for the oxygen reduction reaction (ORR) to replace the state-of-the-art noble metal is essential for commercialization of fuel cells. Fe–N–C-based electrocatalysts are considered as a promising alternative to commercial Pt/C. An efficient electrocatalyst commonly requires large density of active site, high surface area, and desirable porosity, especially multimodal porosity with both large pores for efficient mass transfer and small pores for exposing as many active sites as possible. Herein, a lamellar metal organic framework (MOF) was developed as a precursor to directly achieve such a highly active Fe–N–C electrocatalyst with high surface area and desirable bimodal porosity. The mesopores arising from the special lamellar morphology of MOF benefits efficient mass transfer, and the nanopores resulting from pyrolysis of the MOF makes the majority of active sites accessible to electrolyte and thus effective for ORR. Uniform distribution of active elements N, C, and Fe at the molecular level in MOF precursor ensures abundant well-dispersed highly active sites in the catalyst. As a result, the catalyst exhibited superior ORR electrocatalytic activity and stability to commercial Pt/C. This strategy, using rarely reported lamellar MOF to prepare ORR catalysts with the merits mentioned, could inspire the exploration of a wide range of electrocatalysts from lamellar MOF precursors for various applications.

KEYWORDS: oxygen reduction reaction, nanostructures, electrocatalysis, fuel cells, metal organic frameworks

INTRODUCTION

Alternative energy conversion and storage devices, such as fuel cells and metal–air batteries, are attracting increasing attention due to fast-growing energy demands. Highly active and durable electrocatalysts for the oxygen reduction reaction (ORR) dominate the overall performance and thus the practical application of these systems.¹ Although platinum (Pt)-based materials are the most frequently investigated ORR catalysts due to their superior activity, limited supply and high cost hinder their large-scale commercial applications. It is critical to explore efficient non-noble metal electrocatalysts for the commercialization of fuel cells and metal–air batteries.

Some earth-abundant metal elements (M, such as Fe, Co, Ni, etc.) have been intensively reported to develop nanohybrids, like nanoparticles, nanorods, and nanosheets, which showed considerable catalytic activity for electroreduction of oxygen.^{2–4} You et al.⁵ prepared a Fe–N–C-doped catalyst with excellent ORR performance, methanol tolerance, and stability through a

facile nontemplate approach, in which polystyrene, melamine, and ferric chloride were used as precursors. The excellent ORR activity was attributed to the incorporation of metal-containing active sites onto the conductive carbon matrix. Zhang et al.⁶ have developed a facile method by pyrolyzing polyaniline and iron with addition of urea to improve ORR performance. Even though the performances of these low-cost complexes have been greatly improved in the past decade, their catalytic performance for ORR is still inferior to that of Pt-based catalysts.

At present, recent advancements in ORR suggest that nitrogen-doped carbon nanostructures (NCNs) could work as efficient catalysts of ORR in alkaline fuel cells.^{7–9} Earth-abundant element-derived catalysts (EAEC) with high activity

Received: November 25, 2016

Accepted: January 18, 2017

Published: January 18, 2017

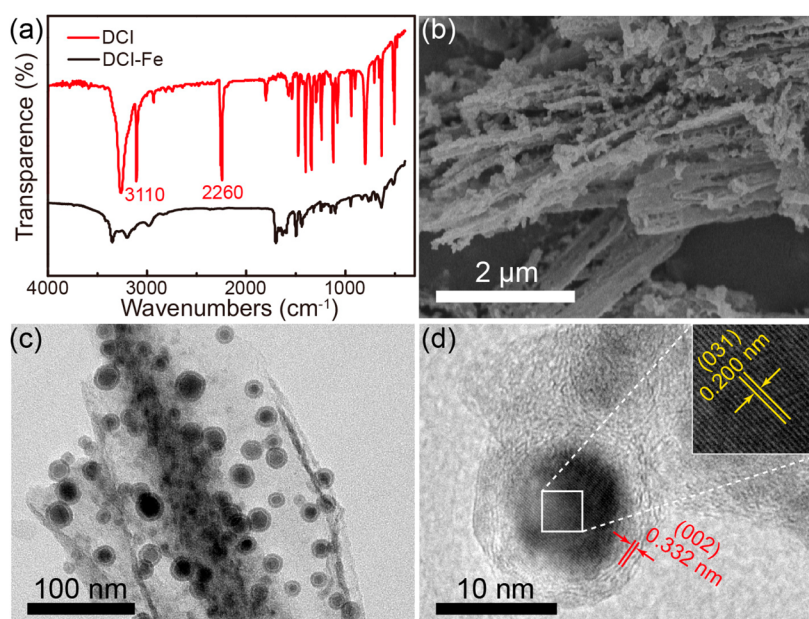
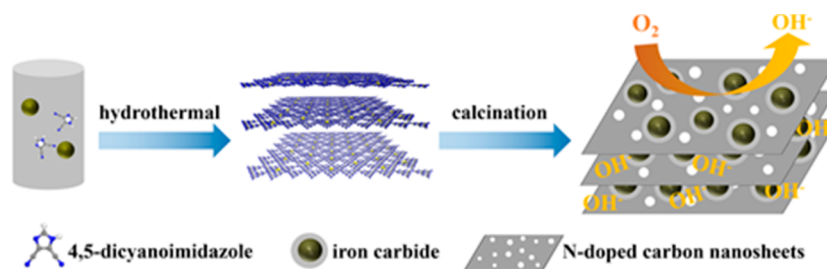
Scheme 1. Schematic Illustration of Preparation of Fe₃C@NC/NCS Nanohybrids

Figure 1. (a) FT-IR spectra for DCI molecule and DCI-Fe MOF. (b) SEM image and (c) TEM image of DCI-Fe-700 catalyst. (d) HRTEM image of Fe₃C@C nanosphere in DCI-Fe-700 catalyst. (Inset) HRTEM image showing lattice fringes of Fe₃C core.

and stability in acid solution are mainly synthesized through pyrolysis of precursors comprising transition metals, nitrogen, and carbon (N-C/M).¹⁰ Recent progress has witnessed a few pyrolyzed N-doped Fe/C catalysts (Fe-N-C) for ORR with excellent activity and stability comparable to and even higher than commercial Pt/C. Carbonaceous, N-containing compounds and iron salts were commonly used as precursors to prepare Fe-N-C catalysts through pyrolysis. Several heterocyclic compounds, such as pyrrole, porphyrins, and phthalocyanines, have also been investigated as precursors.^{11–13}

Generally, interactions among the carbon support, transition metal, and doped nitrogen in the composites play a crucial role in the evolution of active sites conducive to ORR.^{14–16} However, in view of the complexity of the precursors and heterogeneous reactions, it is very challenging to control the structure, morphology, and distribution of Fe-involved active sites due to the high reactivity during high-temperature pyrolysis. Therefore, designing precursors at the molecular level to prepare Fe-N-C electrocatalysts would be an effective way to achieve uniformly distributed active sites and thus superior electrocatalytic performance.

Besides, ORR occurs at a solid-liquid-gas three-phase interface, which requires that the reactants can easily access the active sites of catalysts. Therefore, a hierarchically porous structure with multimodal porosity is highly desirable for ORR, as high microporosity can provide abundant accessible active

sites, while rich mesoporosity is favorable for efficient mass transport in the catalyst layer. Metal organic frameworks (MOF) have shown promising potential in producing ORR catalysts recently, due to their high surface area, nanoporous structure, abundant carbon in building blocks, and well-defined transitional metallic ion center and organic ligands.^{17–28} However, most MOF-based ORR catalysts were derived from three-dimensional bulk MOF crystals with large sizes of micrometers. Compared to that, lamellar MOF exhibits some advantages, such as larger surface area and more accessible active sites on the surface arising from the specific lamellar morphology,²⁹ and lamellar MOF-derived ORR catalysts have rarely been reported.

Herein, we develop a facile and scalable synthetic strategy using the interaction between N-rich dicyanoimidazole (DCI) and iron acetate to prepare a lamellar MOF (named DCI-Fe), which is applied as a precursor to achieve a highly active Fe-N-C electrocatalyst, which consists of well-defined iron carbide nanospheres encapsulated in N-doped carbon shells on N-doped carbon nanosheets (Fe₃C@NC/NCS). The uniform distribution of N, C, and Fe at the molecular level in MOF building blocks ensured the formation of abundant Fe,N-involved highly active sites and their good dispersion on N-doped carbon sheets. Besides, the iron carbide nanospheres are interlaminated in the carbon sheet layers, producing one modal porosity of about 50 nm in the resulting catalysts. The collapse

and carbonization of MOF during pyrolysis produce another modal porosity of about 4 nm. Such a bimodal porosity is beneficial to facilitate mass transfer and provide abundant accessible active sites. As a result, Fe₃C@NC/NCS catalyst exhibited superior electrocatalytic activity and stability for ORR with a half-wave potential of 17 mV, more positive than commercial Pt/C. The present strategy could inspire the development of a wide range of electrocatalysts from lamellar MOF precursors for various applications.

RESULTS AND DISCUSSION

As shown in Scheme 1, Fe₃C@NC/NCS nanohybrids were prepared through a simple and green synthetic method (details given in Experimental Section, Supporting Information). First, by one-pot solvothermal synthesis from 4,5-dicyanoimidazole (DCI) and iron acetate, lamellar organometallic complexes, noted as DCI-Fe, are formed through strong coordinative interaction between metal ions and N atoms in DCI. The DCI-Fe metal organic framework (MOF) was obtained through washing and centrifugation and then was subjected to thermal treatment at a high temperature. Fe₃C nanocrystals encased in N-doped carbon shells were well-dispersed on N-doped carbon nanosheets during the pyrolysis process. The core-shell Fe₃C@NC supported on N-doped carbon nanosheets exhibited extraordinary catalytic activity for ORR. The lamellar MOF precursor was designed to provide bimodal porosity: larger nanopores of tens of nanometers for rapid mass transfer and small nanopores of a couple of nanometers for exposing more active sites. The graphitized nitrogen-doped carbon layers on the surface of Fe₃C nanocrystals can increase the conductivity of the matrix and the chemical stability, thus increasing the durability of catalysts.

The crystalline structure of synthesized DCI-Fe was first examined by X-ray diffraction (XRD). As shown in Figure S1a, DCI-Fe exhibited clear and sharp diffraction peaks, indicating good crystallinity. Due to the strong coordination ability of the imidazole ring of DCI with metal elements, it is expected that MOF is easily formed, which is similar to the formation of widely reported zeolitic imidazole frameworks (ZIFs) from metal and 2-methylimidazole.^{17,28} Then the morphology was characterized by transmission electron microscopy (TEM). As shown in Figure S1b, DCI-Fe MOF exhibited a lateral size of hundreds of nanometers, but the low contrast along the direction of the electron beam suggests its small thickness. Fourier transform infrared (FT-IR) spectroscopy were carried out to verify the conversion from pure DCI to DCI-Fe MOF during the solvothermal process. As shown in Figure 1a, several bands at 1350–1500 and 900–1350 cm⁻¹ for both samples could be ascribed to the stretching and plane vibrations of the imidazole ring, respectively, while the bands below 800 cm⁻¹ could be attributed to out-of-plane vibration of the imidazole ring, among which is the strong band at 636 cm⁻¹ assigned to the C=N stretch mode.³⁰ These results suggest that the linker of imidazole subunits remained unchanged after the formation of DCI-Fe MOF. Notably, strong absorption peaks of the cyano group stretching vibration at 2260 cm⁻¹ and amino stretching vibration at 3110 cm⁻¹ disappeared in the spectrum for DCI-Fe (black curve). However, the new bands at lower wavelength (1590–1700 cm⁻¹) for DCI-Fe are mainly due to formation of N–Fe bonds during the solvothermal procedure, which represent the formation of MOF.³¹ In addition, the appearance of strong absorption bands of DCI-Fe (black curve) at 1500 and 1152 cm⁻¹ may be related to the formation of triazine

rings, indicating that some cyano groups on DCI are trimerized in acidic medium (Fe³⁺ is a classical Lewis acid).³² The new bands of DCI-Fe at 3350 and 3200 cm⁻¹ are assigned to OH and NH₂ groups, respectively, because some cyano groups of DCI are hydrolyzed in the presence of small amounts of water.³³ After heat treatment at 600, 700, and 800 °C, the obtained samples were noted as DCI-Fe-600, -700, and -800, respectively. The morphology of DCI-Fe-700 was examined by scanning electron microscopy (SEM). In Figure 1b, lamellar structures are clearly observed, which are derived from lamellar MOF precursor. Nanoparticles are seen in the interlamination between the layers. The TEM image in Figure 1c illustrates that core-shell structures were supported on lamellar structure. The EDX elemental mapping images of DCI-Fe-700 (Figure S2) clearly show the uniform distribution of Fe, O, and C elements in DCI-Fe-700. The absence of N element was probably due to its low content and the insensitivity of the EDX detector to light elements. The inner nanocrystal cores clearly show the lattice fringes with distance of 0.200 nm in high-resolution transmission electron microscopy (HRTEM, Figure 1d), which was ascribed to the spacing of (031) planes in Fe₃C (JCPDS 35-0772). The clear lattice fringes in the shell part at a distance of 0.332 nm can be well indexed to the spacing of (002) planes in graphitic carbon. However, when the pyrolysis temperature was decreased to 600 °C, no Fe₃C nanocrystals were formed (Figure S3a), which is probably attributed to thermodynamic stabilization of DCI-Fe MOF at 600 °C. The Fe atoms still uniformly dispersed in DCI-Fe-600 through strong coordination bonds in MOF-Fe at this relatively low temperature. When the pyrolysis temperature was increased to 800 °C, the sample (DCI-Fe-800) showed similar core-shell morphology to that for DCI-Fe-700 (Figure S3b) but with a slightly increased diameter of Fe₃C nanocrystals, resulting from the aggregation of nanocrystals under higher pyrolysis temperature.³⁴ The presence of Fe₃C nanocrystals in DCI-Fe-700 and -800 was further confirmed by well-defined diffraction peaks of Fe₃C in their XRD patterns (Figure S4a).³⁵ In addition, DCI-Fe-600 showed no significant peaks, indicating its amorphous nature, further supporting the SEM results. The amorphous nature of DCI-Fe-600 was further supported by the lack of continuous lattice in its HRTEM image and the diffuse rings in the corresponding fast Fourier transform (FFT) image (Figure S5). Raman spectroscopic characterizations of DCI-Fe-600, -700, and -800 samples were carried out to determine the degree of structural defects. The D band stands for a series of structural defects, whereas the G band represents the graphitic structure due to first-order scattering of the E_{2g} mode. In Figure S4b, the intensity ratios of D to G band (I_D/I_G) were determined to be 1.03, 1.02, and 0.91 for DCI-Fe-600, -700, and -800, respectively. The highest I_D/I_G value of DCI-Fe-600 was caused by the lowest degree of graphitization at the lowest temperature. When the temperature was increased to 700 °C, DCI-Fe MOF started to decompose, forming Fe₃C nanocrystals (indicated by XRD patterns). These nanocrystals could catalyze the growth of highly graphitized carbon on their surface, which is the reason for the decrease in I_D/I_G value with increasing pyrolysis temperature.

X-ray photoelectron spectroscopy (XPS) measurements were conducted to elucidate the doping levels and bonding configurations of various samples. Pyrolysis temperature is vital for the structure and composition of resulting materials and thus greatly affects electrocatalytic performance. The nitrogen contents of DCI-Fe-600, -700, and -800 catalysts are

9.98, 7.67, and 3.43 at. %, respectively (Figure 2a and Table S1), indicating nitrogen content decreases with increasing

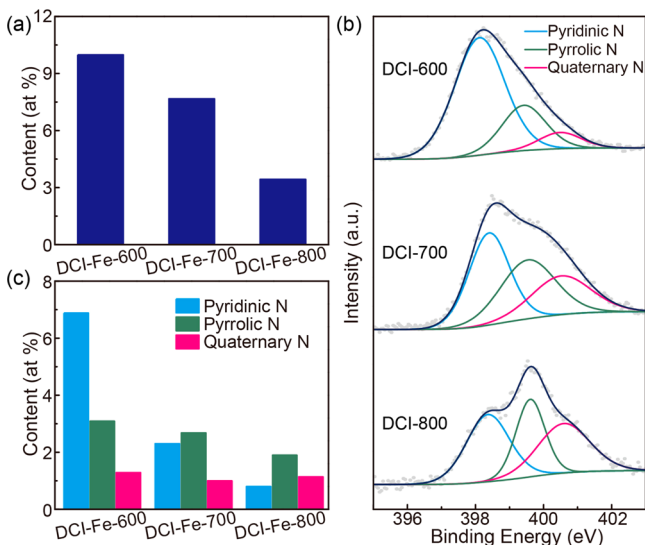


Figure 2. (a) Content of N, (b) high-resolution N 1s peaks in XPS spectra, and (c) content of pyridinic N, pyrrolic N, and quaternary N in DCI-Fe-600, -700, and -800 catalysts.

pyrolysis temperature. This is due to possible decomposition of the bonds between nitrogen and carbon under high temperature, according to previous reports.³⁶ The bonding states of nitrogen could greatly influence the catalytic activity for ORR. Their N 1s spectra were deconvoluted into the components corresponding to pyridinic, pyrrolic, and quaternary nitrogen (Figure 2b).²² The binding energy for each type of nitrogen is summarized in Table S1 and corresponding content is given in Figure 2c. For DCI-600 catalyst, pyridinic N dominates the nitrogen configuration, while for the other two catalysts, the content of pyrrolic N is the highest. This is due to the instability of pyridinic N at higher temperatures. The influence

of pyrolysis temperature on the content of pyridinic N is consistent with a previous report.³⁶ The contents of Fe in DCI-Fe-600, -700, and -800 catalysts were determined to be 49.6, 61.5, and 59.1 wt %, respectively, according to thermogravimetric analysis (TGA) results (Figure S6). The increased content of Fe from DCI-Fe-600 to DCI-Fe-700 is attributed to the greater loss of carbonaceous components during pyrolysis at 700 °C. The slight difference of Fe contents in DCI-700 and DCI-800 means that Fe content remains almost unchanged when the pyrolysis temperature is higher than 700 °C.

Specific surface areas and pore-size distributions of three samples were determined by N₂ adsorption/desorption analysis. The isotherms for DCI-Fe-600, -700, and -800 catalysts exhibited type IV isotherm characteristics (Figure 3a–c), indicative of the presence of mesopores. The Brunauer–Emmett–Teller (BET) surface areas were 85 m²·g⁻¹ for DCI-Fe-600, 249 m²·g⁻¹ for DCI-Fe-700, and 357 m²·g⁻¹ for DCI-Fe-800. The increasing surface area of samples obtained with increasing pyrolysis temperature may be attributed to the decomposition of small organic molecules and to pore evolution, similar to the reported results.³⁶ Nevertheless, DCI-Fe-700 possesses the best configuration and highest content of N element from XPS results, which suggests that the best electrocatalytic performance may be seen on DCI-Fe-700. Pore-size distribution curves for DCI-Fe-600, -700, and -800 catalysts (Figure 3d–f) obviously showed similar mesoporous structure with pore size about 50 nm. Another modal porosity for three catalysts could be observed with pore size about 4 nm, which is attributed to the collapse and carbonization of MOF during pyrolysis. Moreover, the density of this modal porosity increases with increasing pyrolysis temperature, further confirming that formation of the second modal porosity is related to the pyrolysis process. Mesopores with larger size (about 50 nm) could facilitate efficient mass transfer, while nanopores with smaller size (about 4 nm) could provide abundant accessible active sites. Such a bimodal porosity is significantly beneficial for enhancing the electrocatalytic ORR performance of catalysts.

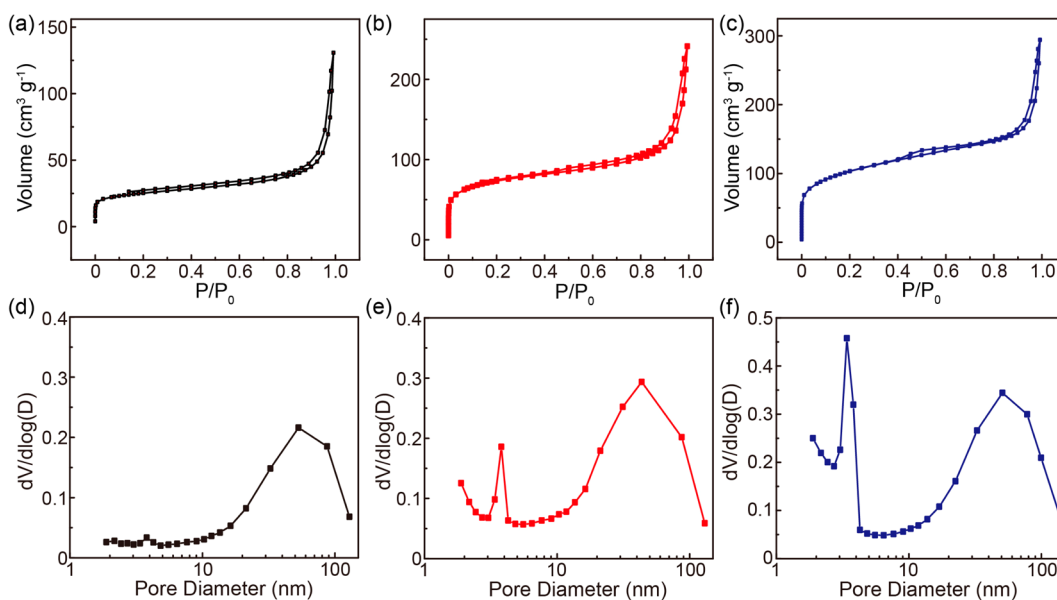


Figure 3. (a–c) N₂ adsorption/desorption isotherms and (d–f) pore-size distribution curves of (a, d) DCI-Fe-600, (b, e) DCI-Fe-700, and (c, f) DCI-Fe-800.

The ORR electrocatalytic activity of DCI-Fe-700 was evaluated by cyclic voltammetry (CV) in 0.1 M KOH solution. As shown in Figure 4a, no obvious redox peaks could be

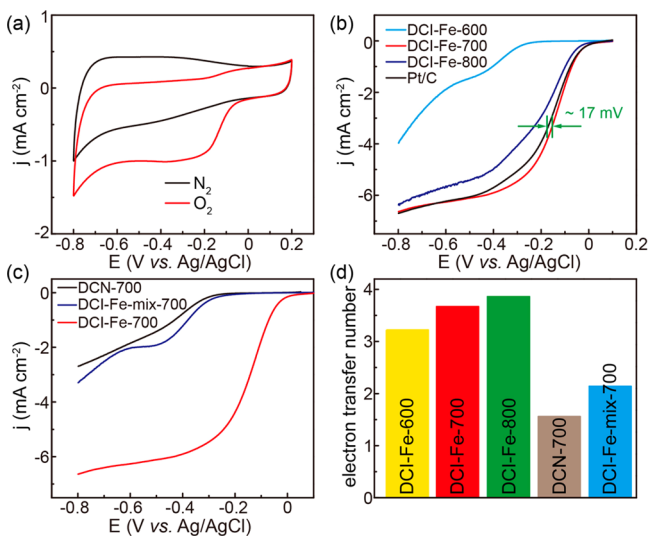


Figure 4. (a) CVs of DCI-Fe-700 in N_2 - and O_2 -saturated 0.1 M KOH solution at a scan rate of $50 \text{ mV}\cdot\text{s}^{-1}$. (b) LSV curves of DCI-Fe-600, -700, and -800 and Pt/C at a rotation rate of 1600 rpm. (c) LSV curves for DCN-700, DCI-Fe-mix-700, and DCI-Fe-700 at a rotation rate of 1600 rpm. (d) Electron transfer numbers of DCI-Fe-600, -700, and -800 catalysts and DCN and DCI-Fe-mix-700 control samples at -0.7 V . The loading of all catalysts, including obtained non-noble materials and commercial Pt/C, is $100 \mu\text{g}\cdot\text{cm}^{-2}$.

identified from CV in N_2 -saturated electrolyte. In contrast, a well-defined oxygen reduction peak centered at -0.18 V was present in O_2 -saturated electrolyte, suggesting excellent ORR electrocatalytic activity. This is further confirmed by the onset potential and diffusion-limited current density on linear sweep voltammetry (LSV) of DCI-Fe-700, comparable to commercial Johnson Matthey Pt/C (Figure 4b). However, DCI-Fe-700 exhibited a half-wave potential ($E_{1/2}$) at -0.152 V , 17 mV more positive than -0.169 V for commercial Pt/C, which suggests more active performance for DCI-Fe-700 than Pt/C. However, DCI-Fe-600 showed a much more negative onset potential, indicating less active properties for ORR. In addition, the catalytic ORR activity of DCI-Fe MOF was also evaluated. As shown in Figure S7, the lamellar MOF itself showed good catalytic ORR activity with a positive onset potential at about -0.18 V , which even is more positive than that for DCI-Fe-600. The catalytic ORR activity of DCI-Fe could come from the inherent Fe–N coordination, further confirming the formation for Fe–N coordination in DCI-Fe MOF. The low limited current density of $3.56 \text{ mA}\cdot\text{cm}^{-2}$ at -0.8 V was probably due to its low conductivity. Although DCI-Fe-600 has the highest nitrogen content (9.98 at. %), it showed the lowest catalytic activity, which is ascribed to the lowest BET surface area ($85 \text{ m}^2\cdot\text{g}^{-1}$). When the pyrolysis temperature was increased to $800 \text{ }^\circ\text{C}$, the onset potential was improved for DCI-Fe-800 but still lower than that for DCI-Fe-700. This is due to the great loss of nitrogen under high temperature, even though DCI-Fe-800 has higher BET surface area than DCI-Fe-700 (357 vs $249 \text{ m}^2\cdot\text{g}^{-1}$). Therefore, it is concluded that pyrolysis temperature has a large influence on the ORR activity of MOF-derived catalysts. The proper temperature, that is, $700 \text{ }^\circ\text{C}$, guarantees the high content of active nitrogen configuration and iron along with

large surface area with bimodal porosity that provides more accessible active sites and facilitates efficient mass transfer. Moreover, the graphitic carbon activated by Fe_3C nanoparticles were believed to be the active site, which gave rise to the catalytic activity.^{37–39} In comparison, two catalysts were prepared via the same method for synthesizing DCI-Fe-700 but without addition of iron acetate (DCN-700) and merely mixing DCI and iron acetate in mortar without formation of MOF precursor (DCI-Fe-mix-700). Their ORR activities were also examined (Figure 4c). The worst performance was observed on DCN-700, indicating the importance of iron during the formation of active sites. The DCI-Fe-mix-700 also showed much lower onset potential and smaller current density than DCI-Fe-700, suggesting the formation of Fe–N bonds in DCI-Fe MOF during the solvothermal process is vital for high catalytic performance. Designing the precursors at molecular level to prepare Fe–N–C electrocatalysts would be an effective way to achieve uniformly distributed active sites and thus superior electrocatalytic performance. To gain further insights into the reaction kinetics on MOF-derived catalysts and control samples, electron transfer number (n) was calculated on the basis of the rotating disk electrode (RDE) measurements with different rotating speeds ranging from 400 to 2000 rpm (Figures S8 and S9). The corresponding Koutecky–Levich (K–L) plots at various potentials showed fairly good linearity, indicating first-order reaction kinetics. The electron transfer numbers at -0.7 V for DCI-600, -700, and -800 are determined to be 3.22, 3.67, and 3.86, suggesting a four-electron-dominated ORR process on the three MOF-derived catalysts and the higher pyrolysis temperature is favorable to the higher electron transfer number (Figure 4d). Otherwise, the control samples showed much lower electron transfer numbers of 1.56 for DCN-700 and 2.14 for DCI-Fe-mix-700, indicating two-electron-dominated ORR process on these two control samples (Figure S10). This result implies that the DCI-Fe MOF precursor could produce electrocatalysts with larger surface area and bimodal porosity due to the uniform distribution of iron element in MOF,⁴⁰ which largely enhancing the electrocatalytic ORR performance.

Fuel crossover is an important issue in fuel cell. Therefore, in addition to high catalytic activity, an ideal ORR catalyst should exhibit satisfactory tolerance to fuel such as methanol. The chronoamperometric curves (Figure 5a) showed that the current density of Pt/C exhibited a sharp reduction after the addition of methanol, while the current density of DCI-Fe-700 remained very steady, suggesting DCI-Fe-700 possesses an excellent tolerance to methanol poisoning effects. Finally, the

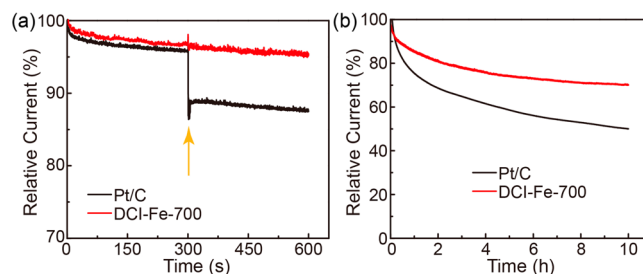


Figure 5. (a) Chronoamperometric response of DCI-Fe-700 and Pt/C catalysts to addition of methanol. The arrow indicates the addition of methanol. (b) Chronoamperometric responses of DCI-Fe-700 and Pt/C catalysts in O_2 -saturated 0.1 M KOH.

stability of DCI-Fe-700 was evaluated by chronoamperometric measurement. As shown in Figure Sb, current density after 10 h test remains 70% for DCI-Fe-700, whereas the value is 51% for commercial Pt/C, indicating the former delivered much better durability. The better durability is ascribed to the protection of Fe₃C nanocrystals by graphitized nitrogen carbide shells.

On the basis of the above structural and compositional characterizations, DCI-Fe-700 presents outstanding electrochemical properties, which can be attributed to the following factors. First, the strong coordination between Fe and DCI and the molecularly uniform distribution of N, C, and Fe in DCI-Fe precursor leads to uniformly distributed N-doped carbon and the carbon nitride-coated Fe₃C core as active sites. The high percentage of pyridinic and pyrrolic N (7.67%) in graphitized shell and nanosheet can promote O₂ adsorption due to increased charge density of the C atoms and also enhance hydrophilicity, strengthening the electrolyte–electrode interaction. Second, the lamellar MOF precursor favors the formation of bimodal porous electrocatalysts with high surface area. The bimodal porosity can simultaneously facilitate mass transfer and provide abundant accessible active sites. Third, the encapsulated metal nanoparticles could lead to a unique host–guest electronic interaction and change the local work function of the carbon nitride shell, making the outer surface of the N-doped carbon layer more active for ORR.^{41,42}

CONCLUSION

In summary, this work reported a facial synthesis of a lamellar metal organic framework (MOF) from solvothermal reaction between iron acetate and dicyanoimidazole, which could be applied to produce an efficient Fe–N–C-based ORR electrocatalyst in the form of carbon shell-encased iron carbides supported on N-doped carbon shell. Such MOF provided molecularly uniform distribution of active elements to form well-dispersed catalytically active sites. The high nitrogen fraction in MOF precursor ensured high nitrogen doping and thus abundant active sites in the catalyst. The bimodal porosity endowed by the special lamellar MOF precursor not only facilitated the mass-transfer process through the mesopores but also guaranteed the high surface area to expose abundant accessible active sites through the nanopores. Benefiting from these features, the resulting catalyst exhibited electrocatalytic performance superior to that of commercial Pt/C for ORR in terms of better activity and stability in alkaline conditions. These results demonstrated the great potential of lamellar MOFs as effective precursors to produce electrocatalysts with desirable structure, which might pave the way to further development of efficient nanomaterials for various applications such as other heterocatalytic reactions, metal–air batteries, and so forth.

ASSOCIATED CONTENT

Supporting Information

The Supporting Information is available free of charge on the ACS Publications website at DOI: 10.1021/acsami.6b15154.

Additional text with experimental details; 10 figures showing XRD and TEM images, EDX elemental mapping, Raman spectra, HRTEM and FFT images, TGA results, and LSV curves and K–L plots; one table listing nitrogen content deconvoluted from N 1s spectra (PDF)

AUTHOR INFORMATION

Corresponding Authors

*E-mail jiangwenjie@iccas.ac.cn (W.-J.J.).

*E-mail wumb@upc.edu.cn (M.W.).

*E-mail hujis@iccas.ac.cn (J.-S.H.).

ORCID

Jin-Song Hu: 0000-0002-6268-0959

Notes

The authors declare no competing financial interest.

ACKNOWLEDGMENTS

We acknowledge financial support from the National Key Research and Development Program of China (2016YFB0101200), the National Key Program on Basic Research (2015CB932302), the National Natural Science Foundation of China (21572269, 21302224, and 21436003), and the Strategic Priority Research Program of the Chinese Academy of Sciences (XDB12020100), Qingdao Science and Technology Plan (15-9-1-108-jch).

REFERENCES

- (1) Yuan, S.; Goenaga, G.; Grabstanowicz, L.; Shui, J.; Chen, C.; Commet, S.; Repogle, B.; Liu, D. J. New Approach to High-Efficiency Non-PGM Catalysts Using Rationally Designed Porous Organic Polymers. *ECS Trans.* **2013**, *58*, 1671–1680.
- (2) Liu, Z. Q.; Cheng, H.; Li, N.; Ma, T. Y.; Su, Y. Z. ZnCo₂O₄ Quantum Dots Anchored on Nitrogen-Doped Carbon Nanotubes as Reversible Oxygen Reduction/Evolution Electrocatalysts. *Adv. Mater.* **2016**, *28*, 3777–3784.
- (3) Wen, Z.; Ci, S.; Zhang, F.; Feng, X.; Cui, S.; Mao, S.; Luo, S.; He, Z.; Chen, J. Nitrogen-Enriched Core-Shell Structured Fe/Fe₃C-C Nanorods as Advanced Electrocatalysts for Oxygen Reduction Reaction. *Adv. Mater.* **2012**, *24*, 1399–1404.
- (4) Ding, W.; Wei, Z.; Chen, S.; Qi, X.; Yang, T.; Hu, J.; Wang, D.; Wan, L. J.; Alvi, S. F.; Li, L. Space-Confinement-Induced Synthesis of Pyridinic- and Pyrrolic-Nitrogen-Doped Graphene for the Catalysis of Oxygen Reduction. *Angew. Chem., Int. Ed.* **2013**, *52*, 11755–11759.
- (5) You, C.; Liao, S.; Qiao, X.; Zeng, X.; Liu, F.; Zheng, R.; Song, H.; Zeng, J.; Li, Y. Conversion of Polystyrene Foam to a High-Performance Doped Carbon Catalyst with Ultrahigh Surface Area and Hierarchical Porous Structures for Oxygen Reduction. *J. Mater. Chem. A* **2014**, *2*, 12240–12246.
- (6) Zhang, J.; Li, Q. D.; Wu, H.; Zhang, C. Y.; Cheng, K.; Zhou, H.; Pan, M.; Mu, S. C. Nitrogen-Self-Doped Carbon with a Porous Graphene-Like Structure as a Highly Efficient Catalyst for Oxygen Reduction. *J. Mater. Chem. A* **2015**, *3*, 10851–10857.
- (7) Yang, S.; Feng, X.; Wang, X.; Müllen, K. Graphene-Based Carbon Nitride Nanosheets as Efficient Metal-Free Electrocatalysts for Oxygen Reduction Reactions. *Angew. Chem., Int. Ed.* **2011**, *50*, 5339–5343.
- (8) Rao, C. V.; Cabrera, C. R.; Ishikawa, Y. In Search of the Active Site in Nitrogen-Doped Carbon Nanotube Electrodes for the Oxygen Reduction Reaction. *J. Phys. Chem. Lett.* **2010**, *1*, 2622–2627.
- (9) Yu, D.; Wei, L.; Jiang, W.; Wang, H.; Sun, B.; Zhang, Q.; Goh, K.; Si, R.; Chen, Y. Nitrogen Doped Holey Graphene as an Efficient Metal-Free Multifunctional Electrochemical Catalyst for Hydrazine Oxidation and Oxygen Reduction. *Nanoscale* **2013**, *5*, 3457–3464.
- (10) Zhao, S.; Yin, H.; Du, L.; He, L.; Zhao, K.; Chang, L.; Yin, G.; Zhao, H.; Liu, S.; Tang, Z. Carbonized Nanoscale Metal-Organic Frameworks as High Performance Electrocatalyst for Oxygen Reduction Reaction. *ACS Nano* **2014**, *8*, 12660–12668.
- (11) Meng, Y.; Voiry, D.; Goswami, A.; Zou, X.; Huang, X.; Chhowalla, M.; Liu, Z.; Asefa, T. N-, O-, and S-Tridoped Nanoporous Carbons as Selective Catalysts for Oxygen Reduction and Alcohol Oxidation Reactions. *J. Am. Chem. Soc.* **2014**, *136*, 13554–13557.
- (12) Yuan, S.; Shui, J. L.; Grabstanowicz, L.; Chen, C.; Commet, S.; Repogle, B.; Xu, T.; Yu, L.; Liu, D. J. A Highly Active and Support-

Free Oxygen Reduction Catalyst Prepared from Ultrahigh-Surface-Area Porous Polyporphyrin. *Angew. Chem., Int. Ed.* **2013**, *52*, 8349–8353.

(13) Jiang, Y.; Lu, Y.; Lv, X.; Han, D.; Zhang, Q.; Niu, L.; Chen, W. Enhanced Catalytic Performance of Pt-Free Iron Phthalocyanine by Graphene Support for Efficient Oxygen Reduction Reaction. *ACS Catal.* **2013**, *3*, 1263–1271.

(14) Wang, Q.; Zhou, Z. Y.; Lai, Y. J.; You, Y.; Liu, J. G.; Wu, X. L.; Terefe, E.; Chen, C.; Song, L.; Rauf, M.; Tian, N.; Sun, S.-G. Phenylenediamine-Based FeN_x/C Catalyst with High Activity for Oxygen Reduction in Acid Medium and Its Active-Site Probing. *J. Am. Chem. Soc.* **2014**, *136*, 10882–10885.

(15) Zhang, S.; Zhang, Y.; Jiang, W.; Liu, X.; Xu, S.; Huo, R.; Zhang, F.; Hu, J.-S. Co@N-CNTs Derived from Triple-Role CoAl-Layered Double Hydroxide as an Efficient Catalyst for Oxygen Reduction Reaction. *Carbon* **2016**, *107*, 162–170.

(16) Zhang, Y.; Huang, L.-B.; Jiang, W.-J.; Zhang, X.; Chen, Y.-Y.; Wei, Z.; Wan, L.-J.; Hu, J.-S. Sodium Chloride-Assisted Green Synthesis of a 3D Fe-N-C Hybrid as a Highly Active Electrocatalyst for the Oxygen Reduction Reaction. *J. Mater. Chem. A* **2016**, *4*, 7781–7787.

(17) Zhong, H.-X.; Wang, J.; Zhang, Y.-W.; Xu, W.-L.; Xing, W.; Xu, D.; Zhang, Y.-F.; Zhang, X.-B. ZIF-8 Derived Graphene-Based Nitrogen-Doped Porous Carbon Sheets as Highly Efficient and Durable Oxygen Reduction Electrocatalysts. *Angew. Chem., Int. Ed.* **2014**, *53*, 14235–14239.

(18) Xiang, Z.; Xue, Y.; Cao, D.; Huang, L.; Chen, J.-F.; Dai, L. Highly Efficient Electrocatalysts for Oxygen Reduction Based on 2D Covalent Organic Polymers Complexed with Non-Precious Metals. *Angew. Chem., Int. Ed.* **2014**, *53*, 2433–2437.

(19) Xia, B. Y.; Yan, Y.; Li, N.; Wu, H. B.; Lou, X. W.; Wang, X. A Metal–Organic Framework-Derived Bifunctional Oxygen Electrocatalyst. *Nat. Energy* **2016**, *1*, 15006.

(20) Zhao, D.; Shui, J.-L.; Grabstanowicz, L. R.; Chen, C.; Commet, S. M.; Xu, T.; Lu, J.; Liu, D.-J. Highly Efficient Non-Precious Metal Electrocatalysts Prepared from One-Pot Synthesized Zeolitic Imidazole Frameworks. *Adv. Mater.* **2014**, *26*, 1093–1097.

(21) Wang, X.; Zhang, H.; Lin, H.; Gupta, S.; Wang, C.; Tao, Z.; Fu, H.; Wang, T.; Zheng, J.; Wu, G.; Li, X. Directly Converting Fe-Doped Metal–Organic Frameworks into Highly Active and Stable Fe-N-C Catalysts for Oxygen Reduction in Acid. *Nano Energy* **2016**, *25*, 110–119.

(22) Shang, L.; Yu, H.; Huang, X.; Bian, T.; Shi, R.; Zhao, Y.; Waterhouse, G. I. N.; Wu, L.-Z.; Tung, C.-H.; Zhang, T. Well-Dispersed ZIF-Derived Co,N-Co-doped Carbon Nanoframes through Mesoporous-Silica-Protected Calcination as Efficient Oxygen Reduction Electrocatalysts. *Adv. Mater.* **2016**, *28*, 1668–1674.

(23) Wei, J.; Liang, Y.; Hu, Y.; Kong, B.; Simon, G. P.; Zhang, J.; Jiang, S. P.; Wang, H. A Versatile Iron–Tannin-Framework Ink Coating Strategy to Fabricate Biomass-Derived Iron Carbide/Fe-N-Carbon Catalysts for Efficient Oxygen Reduction. *Angew. Chem., Int. Ed.* **2016**, *55*, 1355–1359.

(24) Barkholtz, H. M.; Liu, D.-J. Advancements in Rationally Designed PGM-free Fuel Cell Catalysts Derived from Metal–Organic Frameworks. *Mater. Horiz.* **2017**, *4*, 20–37.

(25) Zhang, H.; Osgood, H.; Xie, X.; Shao, Y.; Wu, G. Engineering Nanostructures of PGM-Free Oxygen-Reduction Catalysts Using Metal–Organic Frameworks. *Nano Energy* **2017**, *31*, 331–350.

(26) Li, J.-S.; Li, S.-L.; Tang, Y.-J.; Han, M.; Dai, Z.-H.; Bao, J.-C.; Lan, Y.-Q. Nitrogen-Doped Fe/Fe₃C@Graphitic Layer/Carbon Nanotube Hybrids Derived from MOFs: Efficient Bifunctional Electrocatalysts for ORR and OER. *Chem. Commun.* **2015**, *51*, 2710–2713.

(27) Cho, K.; Han, S.-H.; Suh, M. P. Copper–Organic Framework Fabricated with CuS Nanoparticles: Synthesis, Electrical Conductivity, and Electrocatalytic Activities for Oxygen Reduction Reaction. *Angew. Chem., Int. Ed.* **2016**, *55*, 15301–15305.

(28) Yin, P.; Yao, T.; Wu, Y.; Zheng, L.; Lin, Y.; Liu, W.; Ju, H.; Zhu, J.; Hong, X.; Deng, Z.; Zhou, G.; Wei, S.; Li, Y. Single Cobalt Atoms

with Precise N-Coordination as Superior Oxygen Reduction Reaction Catalysts. *Angew. Chem., Int. Ed.* **2016**, *55*, 10800–10805.

(29) Cao, F.; Zhao, M.; Yu, Y.; Chen, B.; Huang, Y.; Yang, J.; Cao, X.; Lu, Q.; Zhang, X.; Zhang, Z.; Tan, C.; Zhang, H. Synthesis of Two-Dimensional CoS_{1.097}/Nitrogen-Doped Carbon Nanocomposites Using Metal–Organic Framework Nanosheets as Precursors for Supercapacitor Application. *J. Am. Chem. Soc.* **2016**, *138*, 6924–6927.

(30) Yao, J.; Chen, R.; Wang, K.; Wang, H. Direct Synthesis of Zeolitic Imidazolate Framework-8/Chitosan Composites in Chitosan Hydrogels. *Microporous Mesoporous Mater.* **2013**, *165*, 200–204.

(31) Tran, U. P. N.; Le, K. K. A.; Phan, N. T. S. Expanding Applications of Metal–Organic Frameworks: Zeolite Imidazolate Framework ZIF-8 as an Efficient Heterogeneous Catalyst for the Knoevenagel Reaction. *ACS Catal.* **2011**, *1*, 120–127.

(32) Kuhn, P.; Antonietti, M.; Thomas, A. Porous, Covalent Triazine-Based Frameworks Prepared by Ionothermal Synthesis. *Angew. Chem., Int. Ed.* **2008**, *47*, 3450–3453.

(33) Giordano, C.; Kraupner, A.; Fleischer, I.; Henrich, C.; Klingelhofer, G.; Antonietti, M. Non-conventional Fe₃C-based Nanostructures. *J. Mater. Chem.* **2011**, *21*, 16963–16967.

(34) Wu, G.; More, K. L.; Johnston, C. M.; Zelenay, P. High-Performance Electrocatalysts for Oxygen Reduction Derived from Polyaniline, Iron, and Cobalt. *Science* **2011**, *332*, 443–447.

(35) Hu, Y.; Jensen, J. O.; Zhang, W.; Cleemann, L. N.; Xing, W.; Bjerrum, N. J.; Li, Q. Hollow Spheres of Iron Carbide Nanoparticles Encased in Graphitic Layers as Oxygen Reduction Catalysts. *Angew. Chem., Int. Ed.* **2014**, *53*, 3675–3679.

(36) Jiang, W.-J.; Hu, J.-S.; Zhang, X.; Jiang, Y.; Yu, B.-B.; Wei, Z.-D.; Wan, L.-J. In Situ Nitrogen-Doped Nanoporous Carbon Nanocables as an Efficient Metal-Free Catalyst for Oxygen Reduction Reaction. *J. Mater. Chem. A* **2014**, *2*, 10154–10160.

(37) Wu, Z. Y.; Xu, X. X.; Hu, B. C.; Liang, H. W.; Lin, Y.; Chen, L. F.; Yu, S. H. Iron Carbide Nanoparticles Encapsulated in Mesoporous Fe-N-Doped Carbon Nanofibers for Efficient Electrocatalysis. *Angew. Chem., Int. Ed.* **2015**, *54*, 8179–8183.

(38) Deng, D.; Yu, L.; Chen, X.; Wang, G.; Jin, L.; Pan, X.; Deng, J.; Sun, G.; Bao, X. Iron Encapsulated within Pod-like Carbon Nanotubes for Oxygen Reduction Reaction. *Angew. Chem., Int. Ed.* **2013**, *52*, 371–375.

(39) Ren, G.; Lu, X.; Li, Y.; Zhu, Y.; Dai, L.; Jiang, L. Porous Core–Shell Fe₃C Embedded N-Doped Carbon Nanofibers as an Effective Electrocatalysts for Oxygen Reduction Reaction. *ACS Appl. Mater. Interfaces* **2016**, *8*, 4118–4125.

(40) Ma, T. Y.; Dai, S.; Jaroniec, M.; Qiao, S. Z. Metal–Organic Framework Derived Hybrid Co₃O₄-Carbon Porous Nanowire Arrays as Reversible Oxygen Evolution Electrodes. *J. Am. Chem. Soc.* **2014**, *136*, 13925–13931.

(41) Jiang, W. J.; Gu, L.; Li, L.; Zhang, Y.; Zhang, X.; Zhang, L. J.; Wang, J. Q.; Hu, J. S.; Wei, Z.; Wan, L. J. Understanding the High Activity of Fe-N-C Electrocatalysts in Oxygen Reduction: Fe/Fe₃C Nanoparticles Boost the Activity of Fe–N_x. *J. Am. Chem. Soc.* **2016**, *138*, 3570–3578.

(42) Yang, W.; Liu, X.; Yue, X.; Jia, J.; Guo, S. Bamboo-Like Carbon Nanotube/Fe₃C Nanoparticle Hybrids and Their Highly Efficient Catalysis for Oxygen Reduction. *J. Am. Chem. Soc.* **2015**, *137*, 1436–1439.